*Fibre Chemistry, Vol. 44, No. 4, November, 2012 (Russian Original No. 4, September-October, 2012)*

# FIBRE COMPOSITE MATERIALS

## PREPARATION OF BICOMPONENT FIBERS BY SURFACE MODIFICATION WITH FIBROUS CARBON NANOSTRUCTURE FILLER

**A. Yu. Tolbin,* A. V. Nashchokin,***
**A. V. Kepman,* A. P. Malakho,***
**N. E. Sorokina,* V. A. Morozov,***
**V. V. Kulakov,** A. N. Seleznev,***
**and V. V. Avdeev***

UDC 677.019

*Surface treatment of carbon PAN fibers was performed by growing carbon nanostructures using chemical vapor deposition and a mixture of benzene and cyclohexane at 800°C. Fibrous samples with deposited catalyst and with the initial surface were characterized by scanning electron microscopy, Raman scattering, and x-ray phase analysis. Furthermore, the micromechanical characteristics of a model composite monofilament—epoxide matrix were studied using fiber fragmentation. It was found that the resistance to interphase shear for a composite reinforced by surface-treated fiber increased 2.3 times compared with untreated fiber.*

Carbon fibers (CF) surpass all currently known reinforcing fibers and metal alloys with respect to the combination of high specific strength and elastic modulus [1]. Thanks to this, high mechanical characteristics are attained in fibrous polymeric composites in the direction of the reinforcement axis, where the fibers receive the principal mechanical stresses. The transverse and shear strength characteristics of unidirectional carbon plastics have values that are approximately an order of magnitude less than the longitudinal values. Thus, the strength limit for distension in the transverse direction $\sigma_{22}^{+}$, which is equal to the strength limit of the polymeric matrix, is practically never attained.

One of the reasons for the low transverse strength of a unidirectional plastic is the poor adhesive strength of the polymer-matrix bond to the CF surface. Being located in the interfiber space, the matrix receives a part of the mechanical stresses and loses the ability to distribute them among the fibers. As the shear stresses increase, the interphase boundary is destroyed. This causes separation of the CF from the adjoining matrix and destruction of the whole composite [2]. In this instance, the matrix does not determine the integrity of the composite in a highly stressed state. The shear characteristics of composites reinforced with CF are improved substantially as a result of CF surface modification [3].

An effective method for modifying reinforcing CF is aimed at both increasing the interface strength and increasing the rigidity of the surrounding matrix fiber layer. It consists of forming shells of uniformly sized nanostructures on their surface. These are SiC whiskers [4-6] and carbon nanofibers and nanotubes [7]. The large differences in density and thermal expansion coefficients of the components prevents the use of bicomponent fibers based on CF and SiC whiskers as reinforcing filler in the composite. Furthermore, the use of high temperature to produce SiC whiskers (1400°C) and poisonous silane derivatives renders the modification process inefficient from an industrial viewpoint. An alternative

*Lomonosov Moscow State University, 119992, Moscow, 1/1, Leninskie Gory; e-mail: alekseytolbin@gmail.com;**Rubin Aviation Corporation, Balashikha, Moscow Oblast. Translated from *Khimicheskie Volokna*, No. 4, pp. 57-63, September-October, 2012.

 0015-0541/12/4404-0252 

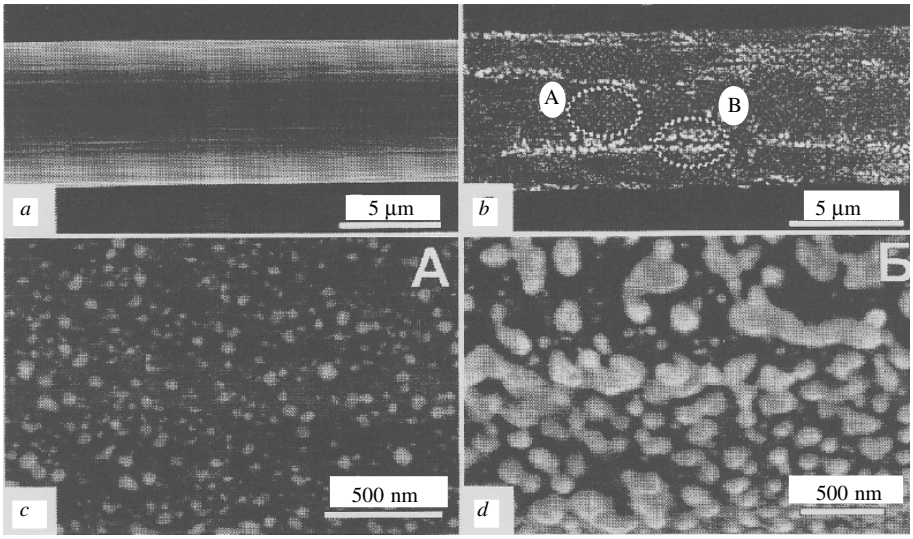


Fig. 1. SEM images of surface condition of initial CF (a) and CF with deposited growth catalyst particles (b). Characteristic regions of catalyst are shown at high magnification by markers A (a) and B (b).

could be modification of the CF surface with unidimensional carbon nanostructures (CNS) by catalytic pyrolysis of hydrocarbons using transition-metal nanoparticles at temperatures <900°C [8, 9].

Methods for preliminary treatment of fiber surfaces that are designed to create a narrow transition-metal nanoparticle-size distribution are known. For this, the fiber surface is functionalized by oxidation in strong acid solutions [10] or in an electrochemical cell [11]. In our instance, CF surface treatment preceding CNS synthesis included deposition of a protective carbon layer based on the $\alpha_2$-fraction of pitch. This prevented the formation of defects involving transition-metal and carbon particles on the CF surface during chemical vapor deposition (CVD) [12]. An additional step for introducing functional groups on the surface was not carried out in order not to complicate the CF modification technology (preparation of bicomponent fiber). Furthermore, it is well known that oxidation destroys the CF subsurface layer and creates additional defects, thereby reducing the fiber strength characteristics [13]. Therefore, a catalyst deposition step and growth of CNS by CVD followed the formation step of the protective layer on the CF surface.

In view of the aforementioned, it was necessary within the scope of the present study to evaluate the nature of the catalyst particle distribution on the CF surface treated with pitch extract; to establish the morphological and structural characteristics of the CNS obtained by CVD; and to compare the contribution of CNS to the formation of the interface between the fiber and the epoxide matrix adjoining it.

We used CF of grade UKN-M based on PAN precursor (monofilament diameter 7.5 ± 0.5 μm). The epoxide finish was removed from the CF surface before the start of the treatment by rinsing the fibers in acetone. An extended bunch of fibers was attached to a metal holder. It should be noted that the fiber rupture strength decreased in this step by 25% relative to finished CF. Then, a protective layer based on the pitch $\alpha_2$-fraction was formed on the CF surface [12]. CNS growth catalyst was deposited on the surface treated in this manner by soaking from a $Ni(NO_3)_2$ solution (0.05 M) in acetone. After this, the holder with the extended fiber was situated in the center of a quartz reactor in the furnace isothermal zone.

The salt deposited on the CF surface was reduced to metal particles in a stream of $H_2$ for 15 min at 400°C before the start of the CVD. The carbon source was an azeotropic mixture of benzene and cyclohexane. The hydrocarbon mixture was supplied by sparging using Ar as a carrier gas. The flow rate of the azeotropic mixture was 4 mL/h. The CVD process was carried out for 30 min at 800°C.

The condition of the CF surface was monitored at various stages of the modification using scanning electron microscopy (SEM) on a microscope with a Quanta 3D FEG field-emission cathode. The accelerating potential was 15 kV; the working section length, ~10 mm.

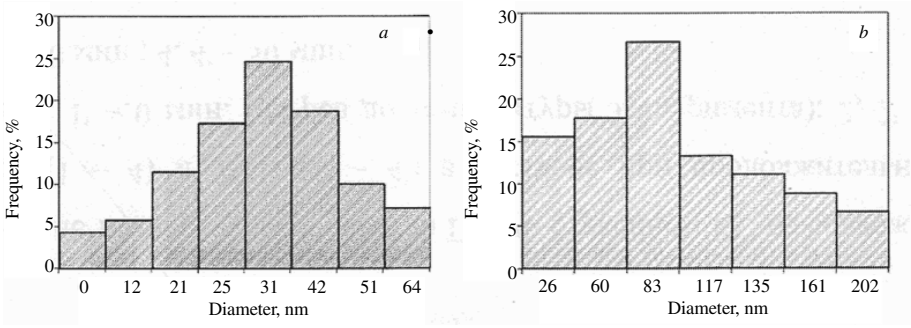


Fig. 2. Size-distribution diagrams of Ni particles in regions A (*a*) and B (*b*).

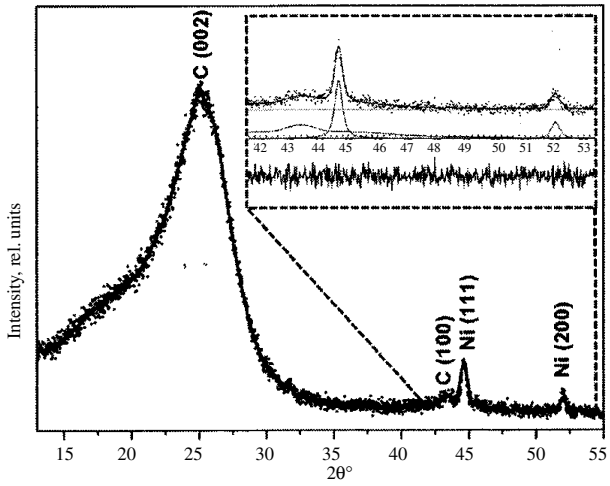


Fig. 3. Diffraction pattern of CF with CNS growth catalyst deposited on the surface. The expanded curve shows peak deconvolution in the range 41-53°.

Figure 1 compares the morphologies of the CF surfaces that were rinsed of finish and CF with deposited catalyst. The Ni particles appeared as white spots on a dark background of C atoms because electrons of the incident beam were reflected better from the heavy-element atoms than from the light C atoms. It can be seen that the catalyst particles covered completely the CF surface. A more detailed examination of the SEM images could identify regions of Ni nanoparticles with average size 31 and 83 nm (Fig. 2) that was calculated from the characteristic regions of the particle distribution (Fig. 1c and 1d). Larger agglomerates of catalyst particles exceeding 100 nm are noticeable.

The Ni particles on the CF surface were compared using x-ray phase analysis. X-ray patterns were obtained at room temperature on a Thermo ARL X-TRA instrument (CuKα-radiation, λ = 1.5418Å, reflection geometry, Peltier semiconducting detector) in scan steps of 1°/min. The diffraction patterns were analyzed using a pseudo-Voigt function and the Fityk program.

The x-ray diffraction patterns (Fig. 3) indicated that a crystalline Ni phase was present. The diffraction patterns showed peaks at 2θ 44.6° and 52.0° with the corresponding *hkl* indices (111) and (200). An analysis of the diffraction peak broadening enabled the size of the coherent scattering region to be determined using the Scherrer equation. According to the calculations, the average size of the Ni crystallites obtained via reduction of $Ni(NO_3)_2$ for 15 min was 28 ± 2 nm. It could be assumed that the large agglomerates of Ni particles that were observed in the SEM were polycrystalline constructs.

In the next modification step, the hydrocarbon mixture was pyrolyzed by the Ni nanoparticles. Figure 4 shows that the CF surface was covered completely by a shell of intertwined CNS fibers of average diameter 38 nm (Fig. 5 shows the distribution diagram). As expected, the diameter of the obtained CNS agreed well with the average diameter of the Ni crystallites. Although the determinations of the particle sizes by SEM were elevated by an average of 21-26% relative

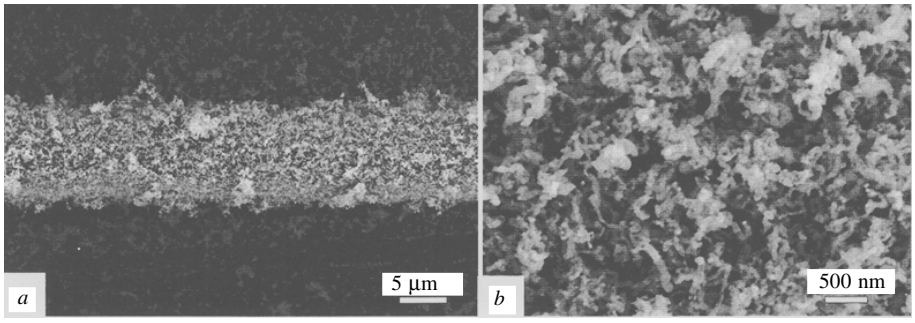


Fig. 4. SEM images of surface modified CF (*a*) and characteristic morphology of CNS grown on CF surface (*b*).

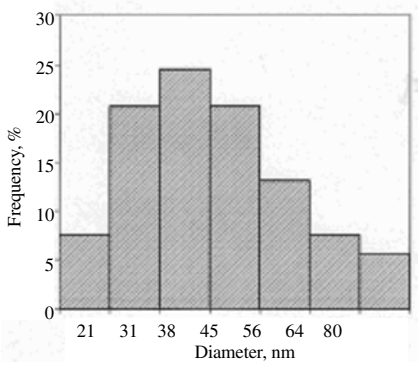


Fig. 5.

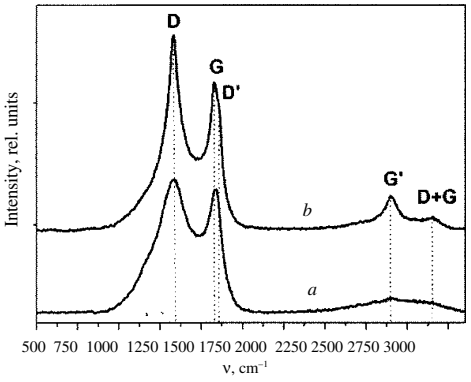


Fig. 6.

Fig. 5. Size-distribution diagram for CNS grown on CF surface.

Fig. 6. Raman spectra: CF with unmodified surface (*a*) and CNS grown on CF surface (*b*).

to the x-ray diffraction data, it should be kept in mind that the coherent scattering region corresponds to the ordered grain region and does not include distorted boundaries and the amorphous interlayer.

Raman scattering (RS) was used to study the structural characteristics of CNS on the CF surface. Raman spectra were recorded using a Renishaw inVia laser Raman spectrometer with excitation by a He—Ne laser operating at wavelength 633 nm. The laser radiation power was 300 mW.

Figure 6 shows the first- (frequency range 1000-1600 $cm^{-1}$) and second-order (2500-3000 $cm^{-1}$) Raman spectra of CF with the initial and modified surfaces. A characteristic feature of first-order Raman spectra of all carbon materials is the presence of *G*-modes at ~1580 $cm^{-1}$. This feature is due to vibrations of C atoms in the plane of the graphene layer [14]. Another feature of first-order Raman spectra is the presence of *D*-modes at ~1350 $cm^{-1}$. This feature appears often in polycrystalline graphite samples. The origin of the vibrations of this mode was associated with symmetry lowering of the ideal graphite layer, with the small sizes of ordered regions, and with the presence of distinct crystallite boundaries [15]. Thus, the ratio of maxima $I_D/I_G$ was indicative of the degree of the graphite structure disorder. The *D′*-mode was observed for the modified fiber as a shoulder on the *G*-mode, which was also correlated with the degree of disordering in carbon materials [14]. This mode was often observed at the edges of graphite planes of highly oriented pyrolytic graphite [16].

An examination of second-order spectra identified the *G′*-mode at 2600 $cm^{-1}$. This corresponded to the first overtone of the *D*-band. Also, a weak band at 2900 $cm^{-1}$ that was the summed overtone of the *D*- and *G*-modes was found. The presence of a resonant enhanced *G′*-mode was known to provide information about the ordering of the graphite layers along the trigonal *c* axis [17] and was not related to defects in the carbon layer structure [18].

We determined the following parameters of the Raman lines for CF with a modified surface based on the results: $\nu_D$ = 1331 $cm^{-1}$, $FWHM_D$ = 76 $cm^{-1}$; $\nu_G$ = 1577 $cm^{-1}$, $FWHM_G$ = 47 $cm^{-1}$; $\nu_{D2}$ = 1610 $cm^{-1}$, $\nu_{G2}$ = 2650 $cm^{-1}$, $FWHM_{D2}$ = 40 $cm^{-1}$, $FWHM_{G2}$ = 137 $cm^{-1}$, $I_D/I_G$ = 1.57.

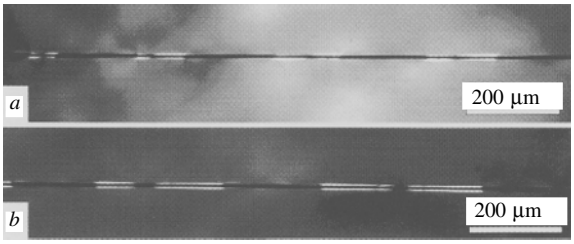


Fig. 7. Optical photographs in polarized light of fragmented fibers with modified (a) and finished (b) surface.

Modes corresponding to the second-order Raman spectrum did not appear for CF with the initial surface. This suggested that an ordered structure was not present in the direction perpendicular to the base plane. The modes *D* ($\nu_D$ = 1333 cm$^{-1}$, $FWHM_D$ = 238 cm$^{-1}$) and *G* ($\nu_G$ = 1587 cm$^{-1}$, $FWHM_G$ = 99 cm$^{-1}$) were strongly broadened although the relative ratio of maxima $I_D/I_G$ = 0.98. The structure of carbon in the CF surface layer could be described with certainty as turbostratic. Resonant enhancement of the *D*-mode relative to the *G*-mode for the modified CF could be related to the content of nonplanar graphene fragments in the CNS that had a strongly twisted thread-like shape.

Thus, it could be stated according to the Raman spectra that the structures of the carbon components included in the surface layer of the starting CF and the CNS prepared on the CF surface were different.

Fiber fragmentation during stretching in the matrix was used to evaluate the adhesive strength of the fibrous filler with the epoxide matrix. The method included preparation of planar dumbbell-shaped samples of thickness 2 mm and working zone length 12 mm. These were single carbon threads located in the epoxide matrix. We used epoxide resin Epikote LR 285 based on bisphenol-A and epichlorohydrin and hardener Epikure LH 287 based on 3,32-dimethyl-4,42-diaminodicyclohexylmethane. The epoxide binder was prepared by mixing the components (resin and hardener) in mass ratio 100:40. The hardening process was carried out at 80°C for 2 h. A stretching load resulting in fragmentation of the fiber was applied to the resulting polymeric fibrous sample. The test was performed on a Tinius Olsen H5KS rupture machine at load rate 5 mm/min. Destruction of the epoxide matrix adjoining the fiber was observed using an Olympus BX51TRF optical microscope in polarized light.

Figure 7 shows examples of deformation—stress patterns for modified and initial CF. The result of fiber fragmentation is shown in them where portions of birefringence are portrayed in white light. This effect was due to the optical sensitivity of the epoxide resin that exhibited optical anisotropy because of the action of mechanical deformation. The polarizability of the polymer macromolecule elementary units became anisotropic because of a shift of the atomic electron shells and the electron clouds forming chemical bonds. Shear stresses leading to an increase of distending stresses up to the strength limit appear when distending forces are applied to the polymer sample with the elemental fiber included in it. In this instance, the elastic energy released upon rupture of the fiber is absorbed by rupture of bonds at the fiber—matrix boundary. This means that the dimensions of the separated part of the fiber upon its destruction in the matrix in addition to the length of the fiber fragment can be estimated from the areas of birefringence (one fragment for the initial CF and three fragments for a modified CF are shown in the optical photographs). Thus, the separation zone upon fragmentation of untreated CF averaged ~130 μm, which was 2.6 times greater than that upon fragmentation of modified CF. A qualitative analysis suggested that a more brittle interface formed between the finished CF and the epoxide matrix.

A quantitative estimate of the interphase interaction of the fiber with the polymer matrix consisted of a determination of the adhesive shear strength ($\tau$) based on the model of Kelly and Tyson [19] regarding the constant shear stress along the working fiber length according to the equation

$$\tau = \frac{\sigma_c}{2(l_c / d)}, \quad (1)$$

where *d* is the CF diameter; $\sigma_c$, the CF strength at the critical fragmentation; $l_c$, the critical CF length determined as the minimal length for which destruction of the CF is possible and the stress reaches the rupture strength limit. It was found

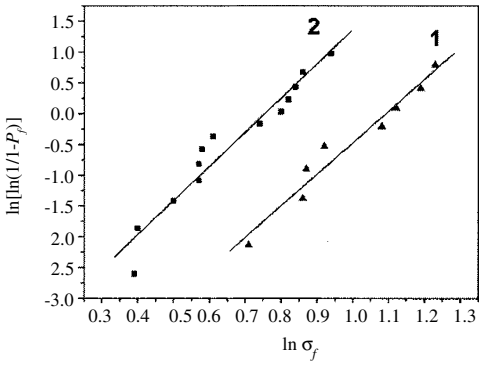


Fig. 8. Plot of Weibull distribution function for finished CF (1) and CF/CNS (2).

Table 1. Micromechanical Tests by Fiber Fragmentation in Polymeric Matrix

| CF type | $m_f$ | $\sigma_c$, GPa | $l/d$ | $\tau$, MPa |
|---|---|---|---|---|
| Initial CF | 5.1 | 5.7±1 | 103±6 | 28±5 |
| CF/CNS | 5.5 | 4.6±0.8 | 35±2 | 65±9 |

empirically that the fragments of destroyed CF were described by a normal distribution. An additional coefficient was introduced to find the critical length [20]:

$$l_c = \frac{4}{3} l_{\text{av}} , \tag{2}$$

where $l_{\text{av}}$ is the average length of a fragment of the destroyed fiber in the matrix. The parameter $\sigma_c$ was found from statistical analysis of mechanical data [21] using a double parametric Weibull equation:

$$\ln\left[\ln\left(\frac{1}{1-P_f}\right)\right] = m_f \ln\left(\sigma_f\right) - m_f \ln\left(\sigma_0 L^{-1/m_f}\right), \tag{3}$$

where $\sigma_f$ is the rupture strength limit of an elementary fiber as determined according to the ISO 11566:1996 standard if the fiber working length is taken as 25 mm; $P_f$, the probability of the event determined as the ratio of the experiment ordinal number to the total number of experiments; $\sigma_0$, the Weibull scale parameter; $m_f$, the Weibull shape parameter; and $L$, the fiber base length, equal to 25 mm.

A function in logarithmic coordinates was constructed for each fiber type. Then, it was analyzed by linear regression to find the Weibull distribution parameters (Fig. 8). The parameter $m_f$ was found from the slope of the resulting lines. Its value was substituted into the formula for determining the critical rupture strength $\sigma_c$:

$$\sigma_c = \sigma_f \left(\frac{l_c}{l_0}\right)^{-1/m_f} . \tag{4}$$

Table 1 presents the parameters of the statistical processing of the fiber rupture mechanics and the values of the adhesion strength that were calculated from test results of fiber fragmentation with modified (CF/CNS) and finished surfaces upon stretching of the polymer composite. It should be noted that parameter $m_f$ characterizes the distribution of defects along the fiber surface and reflects strength variations along its length [22]. The greater parameter $m_f$ is, the less defective the fiber is. The slopes obtained by us were commensurate among themselves, which suggested that the arrays of defects were similar. Because our method of modifying the CF surface did not introduce new types of defects, it is justifiable to compare the adhesion shear strength after modifying the CF surface.

The results suggested that the fiber—epoxide matrix adhesion strength increased after modification by 2.3 times compared with the finished fiber. The critical CF length (~700 μm) after modification was almost three times

greater than the critical length of the starting CF. This was explained by the fact that the weak bond between the components of the reinforced polymer could not provide an effective redistribution of shear stresses through the matrix to the fiber. In this instance, the high CF strength characteristics in the composite could not be fully utilized. Separation of the CF from the matrix would be the most favored process from an energetic viewpoint upon application of a distending load to the polymer composite.

Because the CF surface was not functionalized as a result of the modification and the resulting CNS were lyophobic with respect to the epoxide resin, it could be assumed that the generation of bonding forces at the fiber—matrix interface was related to an increased interfacial area. Then, adhesive contact between the modified CF and the epoxide binder was probably due to its penetration through capillary forces into the space between the thread-like CNS situated orthogonal to the fiber axis. This resulted in the formation of a stronger interface compared with the finished CF.

*The work was carried out with financial support from the Russian Ministry of Education and Science according to Decree of the RF Administration of April 9, 2010, No. 218 "On measures for state support of the development of cooperation between Russian institutions of higher education and organizations performing complex projects on the creation of high-technology production."*

**REFERENCES**

1. S. Chand, *J. Mater. Sci.*, **35**, 1303-1313 (2000).
2. L. T. Drzal, *Adv. Polym. Sci.*, **75**, 1-32 (1986).
3. L. G. Tang and J. L. Kardos, *Polym. Compos.*, **18**, 100-113 (1997).
4. W. Kowbel, C. Bruce, et al., *Composites, Part A*, **28**, 993-1000 (1997).
5. J. V. Milewski, R. G. Shaver, and J. C. Withers, *Mater. Eng.*, **67**, 62 (1968).
6. G. Emig, N. Popovska, et al., *J. Mater. Sci.*, **31**, 4395-4399 (1996).
7. H. Qian, E. S. Greenhalgh, et al., *J. Mater. Chem.*, **20**, 4751-4762 (2010).
8. C. C. Luhrs, D. Garcia, and M. Tehrani, *Carbon*, **47**, 3071-3078 (2009).
9. Z. Fan, C. Wu, and J. Chen, *Carbon*, **46**, 365-389 (2008).
10. Y. Xia, L. Zeng, and W. Wang, *Appl. Surf. Sci.*, **253**, 6807-6810 (2007).
11. M. F. De Riccardis, D. Carbone, et al., *Carbon*, **44**, 671-674 (2006).
12. A. Yu. Tolbin, A. V. Nashchokin, et al., *Khim. Volokna*, No. 1, 22-26 (2012).
13. Z. Wu, C. U. Pittman, et al., *Carbon*, **33**, 597-605 (1995).
14. R. J. Nemanich and S. A. Solin, *Phys. Rev. B: Condens. Matter Mater. Phys.*, **20**, 392-401 (1979).
15. M. S. Dresselhaus, A. Jorio, and R. Saito, *Annu. Rev. Condens. Matter Phys.*, **1**, 89-108 (2010).
16. P. H. Tan, S. Dimovsky, and Yu. Gogotsi, *Philos. Trans. R. Soc. London*, **362**, 2289-2310 (2004).
17. A. C. Ferrari, *Solid State Commun.*, **143**, 47-57 (2007).
18. E. F. Antunes, A. O. Lobo, et al., *Carbon*, **44**, 2202-2219 (2006).
19. A. Kelly and W. R. Tyson, *J. Mech. Phys. Solids*, **13**, 329-350 (1965).
20. D. Tripathi and F. R. Jones, *J. Mater. Sci.*, **33**, 1-16 (1998).
21. I. J. Beyerlein and S. L. Pheonix, *Compos. Sci. Technol.*, **56**, 75-92 (1996).
22. K. Naitoa, Y. Tanaka, et al., *Carbon*, **46**, 189-195 (2008).